

Grid-ECO: Grid Aware Electric Vehicle Charging Stations Placement Optimizer

Bikram Panthee, *Member, IEEE*, Haoming Yang, Corey D. Harper, Amritanshu Pandey *Senior Member, IEEE*

arXiv:2602.12473v1 [eess.SY] 12 Feb 2026

Abstract—The paper develops a methodology, Grid-ECO, to optimally allocate electric vehicle charging stations (EVCS) within a distribution feeder, while considering EV charging demand at census-level granularity. The underlying problem is NP-hard and requires satisfying nonlinear, nonconvex, three-phase unbalanced AC network constraints while including integer decision variables. Existing works cannot guarantee AC feasibility nor optimality of this problem without either i) relaxing the integer decision variable space or ii) convexifying AC constraints. Proposed Grid-ECO exactly solves the underlying mixed-integer nonlinear program (MINLP) to near-zero optimality gap while prioritizing candidate locations based on grid voltage and current sensitivities. To solve the MINLP exactly, Grid-ECO exactly reformulates it into Mixed-Integer Bilinear Program (MIBLP), enabling global optimization using the spatial branch-and-bound algorithm (sBnB). To ensure computational tractability for large-scale feeders, we develop and include a novel presolving strategy based on Sequential Bound Tightening (SBT) with variable filtering and decomposition. Case studies demonstrate that Grid-ECO outperforms the off-the-shelf Gurobi sBnB solver by solving cases where no feasible solution is found within 167 hours. When feasible solution is found by off-the-shelf solver, Grid-ECO reduces solution time by up to 73% and sBnB node exploration by up to 97%, while achieving a 0% optimality gap and guaranteed AC feasibility.

Index Terms—AC network constraint, electric vehicle charging station, Grid-ECO, grid sensitivity, mixed-integer nonlinear program, sequential bound tightening, spatial branch-and-bound.

ACRONYMS AND NOMENCLATURE

TABLE I
ACRONYMS

| | |
|-------|---|
| EVCS | Electric Vehicle Charging Station |
| EV | Electric Vehicle |
| MINLP | Mixed-Integer Nonlinear Program |
| MIBLP | Mixed-Integer Bilinear Program |
| MIQCP | Mixed-Integer Quadratically Constrained Program |
| NLP | Nonlinear Program |

I. INTRODUCTION

The adoption of electric vehicles (EVs) is rapidly increasing, with EV sales in the United States reaching approximately 1.6 million in 2024 and projected to approach 9.6 million by 2030 [1]. Supporting this growth would require a substantial expansion of public EV charging infrastructure, which may place significant stress on existing electric distribution grid networks. In particular,

B. Panthee and A. Pandey are with the Department of Electrical and Biomedical Engineering, University of Vermont, Burlington, VT 05405, USA ({bpanthee,apandey1}@uvm.edu).

H. Yang and C. Harper are with the Department of Civil and Environmental Engineering, Carnegie Mellon University, Pittsburgh, PA 15213, USA ({haomingy,cdharper}@andrew.cmu.edu).

TABLE II
SETS AND VECTORS

| | |
|---------------|--|
| \mathcal{B} | Set of census blocks |
| \mathcal{F} | Set of census blocks in the selected feeder |
| \mathcal{K} | Set of nodes, $\{1,2,\dots,k,\dots\}$ |
| \mathcal{L} | Set of candidate nodes for EVCS placement |
| Φ | Set of phases, $\{A,B,C\}$ |
| \mathcal{T} | Set of transformers |
| \mathbf{s} | Vector of bilinear variables |
| \mathbf{x} | Vector of binary decision variables |
| \mathbf{y} | Vector of AC network variables |
| \mathbf{z} | Vector of positive integer decision variables |
| \mathbf{d} | Vector of charger demand for each census block |

TABLE III
GRID IMPACT INDEX PARAMETERS

| | |
|------------------------------------|---|
| $V_{k\Omega}, \hat{V}_{k\Omega}$ | Voltage at node k , phase Ω , before and after perturbation |
| $V_{k\Omega}^L, V_{k\Omega}^U$ | Min./max. voltage at node k , phase Ω |
| $\Delta V_{k\Omega}^{\delta_{lp}}$ | Voltage deviation at node k , phase Ω due to perturbation at l,p |
| δS_{lp} | Perturbation load at node l , phase p |
| $\Delta I_{\tau}^{\delta_{lp}}$ | Current deviation in transformer τ due to perturbation at l,p |
| I_{τ}, \hat{I}_{τ} | Current in transformer τ before and after perturbation |
| I_{τ}^{rat} | Current rating of transformer τ |
| γ | Penalty factor |

TABLE IV
OPTIMIZATION VARIABLES

| | |
|--|--|
| V_{kp}^r, V_{kp}^i | Real and imaginary voltage at node k , phase p |
| $G_{kp}^{\text{ch}}, B_{kp}^{\text{ch}}$ | Chargers conductance/susceptance at node k , phase p |
| $P_{kp}^{\text{ch}}, Q_{kp}^{\text{ch}}$ | Chargers active/reactive power at node k , phase p |
| $P_{kp}^{\text{load}}, Q_{kp}^{\text{load}}$ | Power demand <i>without</i> EVCS at node k , phase p |
| $G_{kp}^{\text{load}}, B_{kp}^{\text{load}}$ | Load conductance/susceptance at node k , phase p |

ad-hoc placement of electric vehicle charging stations (EVCSs) can lead to transformer overloading, excessive voltage drops, and overall grid instability. Consequently, identifying *where* charging activities occur, along with the corresponding electricity demand [2], becomes a critical design consideration. This observation

motivates the following research problem: *How to identify optimal EVCS locations and charger counts from a set of candidate sites by maximizing charger allocation given a limited budget, grid physics, and census-level charger demand?* To answer this, we first estimate EV charging demand using a transportation modeling framework based on real-world data such as EV adoption, parking availability, and demographic characteristics, and then use this demand as input to a distribution feeder modeling framework. We then solve an optimization problem subject to grid physics and budget constraints to satisfy the estimated charging demand and identify the optimal EVCS locations and associated charger counts.

While accurate demand estimation is generally a prerequisite for EV charging infrastructure planning, charging demand is often estimated at an aggregation level that is not directly compatible with feeder-level grid-aware optimization [3]. In contrast, when demand is estimated at an appropriate spatial resolution, AC power network constraints are typically not considered (e.g., [4], [5]). For instance, Moon et al. [6] utilize discrete choice experiments to analyze consumer preferences and temporal load shifting to estimate charging demand at the national level, effectively bypassing the specific constraints of local electric distribution networks. Wang et al. [7] utilize high-resolution vehicle trajectory data with deep learning techniques, but their objective is short-term temporal forecasting for grid stability rather than identifying optimal locations for long-term infrastructure deployment. More recent agent-based approaches, such as [8], successfully model granular spatial demand at the Traffic Analysis Zone (TAZ) level to optimize service coverage; however, they do not incorporate AC network constraints, limiting their applicability for grid-aware planning.

Granular spatial demand models can estimate the total EV charging demand at the distribution feeder level; however, utility planners must ensure that the allocation of EVCSs and the deployment of charging capacity within a feeder do not violate grid physics and continue to maintain grid health. Consequently, the planning problem requires solving an optimization model that allocates EVCSs and deploys chargers while satisfying AC network constraints, meeting total charging demand, and preserving reliable grid operation. The EVCS allocation and charger deployment problem is inherently discrete, as it involves binary decisions on whether to install an EVCS at a candidate location and integer decisions on the number of chargers to deploy at that location. In addition, the inclusion of AC network constraints introduces nonlinearity and nonconvexity, resulting in a MINLP formulation. The combination of discrete decisions and nonlinear power flow equations makes such problems computationally challenging to solve [9].

Z. Liu et al. [10] proposed a two-step screening method that considers environmental factors and service radius to identify candidate EV charging station locations. They then determine the optimal sizes of these stations by solving a nonlinear optimization problem with AC network constraints. However, this sequential approach may yield suboptimal locations and sizes, since the model does not jointly consider all relevant constraints—such as grid physics, budget limits, charging demand, and anti-clustering—within a single optimization framework. Moreover, the resulting nonconvex problem is solved using a primal–dual interior-point algorithm, which does not guarantee global optimality. In [11], a nonlinear three-phase unbalanced network model was linearized to address the electric vehicle charging scheduling problem, demonstrating a piecewise linearization tech-

nique to relax AC network constraints. Due to linearization, voltage and flow violation representation are not accurate. In [12], a mixed-integer linear model was proposed to place EV charging stations in highway networks with the objective of minimizing the number of charging stations. The proposed model considers the charging demand to be satisfied only by renewable generators and doesn't account for the grid network equations. In [13], the authors solve the mixed-integer linear program by applying convex relaxations to the AC network constraints in order to minimize the total cost of charging stations and protection device upgrades. In [14], the voltage impact matrix is used as an index to assess how the addition of charging stations in specific locations affects the grid. These locations are then categorized as either better or worse based on their impact. However, it is important to note that the selected locations may be suboptimal or infeasible because they were not identified by solving an optimization model that accounts for the grid's operating conditions and physical constraints. Also, they studied only the impact of node voltages, whereas line and transformer loading, which also have a major impact on distribution grid reliability, were not included. In [15], the optimal allocation of charging stations for a bus-route planning problem is formulated as a mixed-integer second-order cone program by relaxing AC network constraints and coupling the power and transportation networks. However, the study considers grid expansion for placing fast charging stations along bus routes, rather than level-2 public charging stations within an urban distribution network.

Despite these contributions, existing works do not comprehensively solve the problem. They either (i) exclude census-level demand, which is required to estimate charger demand and determine locations at the distribution feeder level; (ii) neglect grid physics or rely on relaxed models; or (iii) relax integer decision variables by their continuous approximations. **Grid-ECO** addresses these research gaps by innovating along the following research contributions:

- **Transportation and distribution model integration.** We integrate census block-level EV charging demand derived from a transportation modeling framework as an input into a grid-aware optimization model with exact nonlinear, nonconvex AC distribution network constraints to ensure grid-feasible charger deployment.
- **Candidate location prioritization.** Development of a grid-sensitivity-based prioritization that extends the bus voltage sensitivity approach in [14] by incorporating transformer current flow sensitivities to rank various candidate locations within the Grid-ECO optimization framework.
- **Solving MINLP to near-zero optimality gap.** Extension of the presolving routines in [16] to include integer variables to solve the non-convex MINLP to a near-zero optimality gap, for large-scale feeders in a practical amount of time.

We validate the proposed framework on *two locations within the study region, Seattle, WA*, using census block-level charging demand, which is derived from real-world demographic and transportation data and mapped to the distribution feeder. The results show that the resulting MIBLP (exact reformulation of MINLP) solves to a near-zero optimality gap (see Section V).

II. GRID-ECO PRELIMINARIES

A. Informal Grid-ECO Problem

- **Given:** Transportation model and distribution grid model
- **Output:** Optimal EVCS locations and optimal number of chargers at each selected location
- **Key algorithms:** EV charging demand estimation, candidate location selection, candidate location prioritization, MINLP optimization routine

The *transportation model* input includes the number of EVs and vehicle registrations, household income, race distribution, and parking accessibility to estimate the charging demand in the study region. The *distribution grid model* input includes the network topology, configuration, and load profiles (including existing EVCS). The EV charging demand estimation algorithm (see Section II-B) estimates the net charging demand at the census-block level for the selected study region. The candidate location selection and prioritization algorithms (see Section II-C) identify and prioritize candidate locations. The optimization routine (see Sections III and IV) formulates the MINLP and solves it using the proposed methodology.

B. Charging Demand Modeling

Optimal allocation of EVCS depends on charging demand. We determine the city-wide spatial distribution of EV charging demand using a bi-objective mixed-integer linear programming (MILP) framework, building on work in [17]. The model outputs the optimal number of charging ports in each census block $i \in \mathcal{B}$, denoted by d_i . We sum the net charging demand for all census blocks in the feeder as input for the downstream optimization routine.

The charging demand modeling framework maximizes a weighted combination of utilization efficiency and equitable accessibility, formulated as follows:

$$\max_{\mathbf{d}} \quad (1-\alpha) \sum_{i \in \mathcal{B}} d_i \mu_i + \alpha \sum_{i \in \mathcal{B}} d_i \epsilon_i \quad (1a)$$

$$\text{s.t.} \quad d_i \leq c_i \quad \forall i \in \mathcal{B}, \quad (1b)$$

$$\sum_{i \in \mathcal{B}} d_i = b \quad (1c)$$

In this formulation, the primary decision variable d_i represents the number of charging ports to be allocated to census block i . The objective function (1a) is designed to balance two competing goals. The first component is the near-term demand score μ_i , which reflects expected charger utilization intensity. This score aggregates normalized measures of vehicle density, high-income households, and local EV adoption rates, prioritizing areas with strong indicators for immediate charger use. The second component is the equity need score ϵ_i , which represents the socio-economic necessity for public charging access to support long-term, equitable EV adoption. This score considers factors such as the proportion of minority and low-income households, along with the number of households that lack access to off-street parking. The weighting parameter $\alpha \in [0,1]$ serves as a policy lever to adjust the balance between prioritizing near-term demand (efficiency) and long-term equity needs (accessibility), with $\alpha=0.85$ representing equal weighting for both equity and demand.

The model is bound by two key constraints. Constraint (1b) ensures that the number of charging ports d_i in any given block i does not exceed its transportation infrastructure capacity c_i , such

as available curbside space. Constraint (1c) enforces that the sum of all allocated chargers across all census blocks equals b , which represents the total number of chargers to be deployed city-wide, as dictated by a predefined number of charging ports normalized per 1000 households.

The outcome of this optimization is $\mathbf{d} = [d_1, d_2, \dots, d_i]$, which represents the spatially distributed charging demand for each census block. The total charging demand within the feeder is denoted by D and is calculated as the sum of d_i over all census blocks \mathcal{F} contained in the selected feeder, i.e.,

$$D = \sum_{i \in \mathcal{F}} d_i \quad (2)$$

We show the output charging demand, for $\alpha=0.85$ for Seattle, WA, in Fig. 1. The figure shows the number of new charging ports to be allocated to each census block in the region, given a budget of 5 ports per 1,000 households. Additional details of the formulation of the EV siting and sizing module can be found in [17].

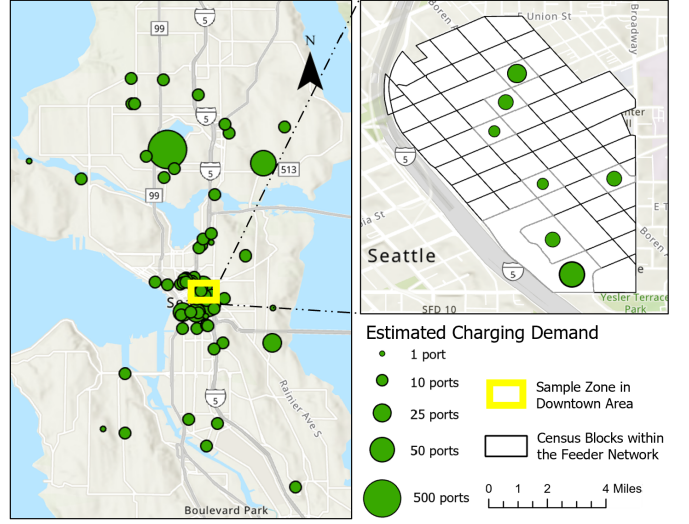


Fig. 1. Estimated EV charging port demand in Seattle, WA ($\alpha=0.85$, 5 ports per 1,000 households). Green circles indicate census-block-level charging demand, with size proportional to the number of ports. The zoomed region shows the selected feeder in downtown Seattle.

C. Candidate Location Selection and Prioritization

We select candidate locations in the distribution grid based on available transformer capacity. Specifically, candidate locations correspond to pole locations with sufficient remaining transformer capacity. The resulting candidate set is larger than the set of census blocks where charging demand is currently estimated, accounting for areas where charging demand will emerge as EV penetration increases, as illustrated in Fig. 3.

We prioritize candidate locations to achieve two objectives: minimizing future impacts on the electrical grid and breaking symmetry in the optimization problem to improve convergence. Many existing distribution grids already operate close to their limits; therefore, adding new loads from EVCS may violate operating constraints on electrical parameters (such as nodal voltages, line power flows, and transformer loading). To assess these impacts, we evaluate the sensitivity of these electrical parameters to the addition of new load, and use the resulting sensitivity measures to identify and prioritize candidate locations.

To quantify this sensitivity, we introduce the Grid Impact Index (GI-index), f^g . A higher GI-index indicates a location is highly sensitive (i.e., results in larger variation of electrical parameters) to load injection, while a lower value indicates a less-sensitive location preferable for charging stations (see Fig. 2). We define the GI-index as a linear combination of the voltage impact index (VI-index) and the current impact index (CI-index), computed via iterative power flow simulations.

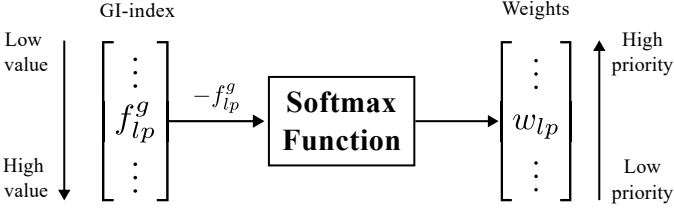


Fig. 2. Softmax-based transformation of the Grid Impact Index into priority weights for candidate location selection.

Voltage and current impact indices: Adapting the work of Zhu *et al.* [18], we define the voltage impact (VI-index), f_{lp}^v , for a candidate node $l \in \mathcal{L}$ at phase $p \in \Phi$ as the normalized sum of voltage deviations across all nodes $k \in \mathcal{K}$ (where $\mathcal{L} \subseteq \mathcal{K}$) and phases $\Omega \in \Phi$, resulting from a unit charger apparent power injection δS_{lp} on node l and phase p :

$$f_{lp}^v = \frac{1}{\delta S_{lp}} \sum_{k \in \mathcal{K}} \sum_{\Omega \in \Phi} \Delta V_{k\Omega}^{\delta_{lp}} \quad (3)$$

We compute the net voltage deviation, ΔV , by combining the absolute voltage deviation $|\hat{V}_{k\Omega} - V_{k\Omega}|$, where $V_{k\Omega}$ and $\hat{V}_{k\Omega}$ denote the voltage magnitude before and after perturbation, with penalty functions ($\min(0, \hat{V}_{k\Omega} - V_{k\Omega}^L)$ and $\min(0, V_{k\Omega}^U - \hat{V}_{k\Omega})$) that activate when the perturbed voltage violates the lower and upper voltage limits ($V_{k\Omega}^L$ and $V_{k\Omega}^U$). These violations are scaled by a penalty factor (γ) to assign higher impact to nodes experiencing limit violations:

$$\Delta V_{k\Omega}^{\delta_{lp}} = |\hat{V}_{k\Omega} - V_{k\Omega}| + \gamma |\min(0, \hat{V}_{k\Omega} - V_{k\Omega}^L) + \min(0, V_{k\Omega}^U - \hat{V}_{k\Omega})| \quad (4)$$

Similarly, we define the CI-index (f_{lp}^c) as the sum of net current deviations, $\Delta I_{\tau}^{\delta_{lp}}$, across all transformers $\tau \in \mathcal{T}$:

$$f_{lp}^c = \frac{1}{\delta S_{lp}} \sum_{\tau \in \mathcal{T}} \Delta I_{\tau}^{\delta_{lp}} \quad (5)$$

where,

$$\Delta I_{\tau}^{\delta_{lp}} = (|(\hat{I}_{\tau} - I_{\tau})| + \gamma |\min(0, I_{\tau}^{\text{rat}} - \hat{I}_{\tau})|) \quad (6)$$

We stack the computed VI-index and CI-index into the VI-index vector f^v and the CI-index vector f^c , for all locations (l,p) respectively.

Grid impact index calculation: To ensure unit consistency, we normalize the vectors of the voltage and current indices, f^v and f^c , by their respective maximum values: $f_{lp}^{n,v} = f_{lp}^v / \max(f^v)$ and $f_{lp}^{n,c} = f_{lp}^c / \max(f^c)$. We then compute the GI-index as:

$$f_{lp}^g = a_{lp} \cdot f_{lp}^{n,v} + b_{lp} \cdot f_{lp}^{n,c} \quad (7)$$

We compute the weights a_{lp} and b_{lp} in (8) proportionally so that the dominant impact determines the index.

$$a_{lp} = \frac{f_{lp}^{n,v}}{f_{lp}^{n,v} + f_{lp}^{n,c}}, \quad b_{lp} = \frac{f_{lp}^{n,c}}{f_{lp}^{n,v} + f_{lp}^{n,c}} \quad (8)$$

Weight Assignment: Finally, to favor locations with low grid impact, we assign prioritization weights w_{lp} , for all locations (l,p) , using the negative softmax function on the GI-index. This approach, illustrated in Fig. 3, assigns higher weights to lower GI-index values:

$$w_{lp} = \text{softmax}(-f_{lp}^g) = \frac{\exp(-f_{lp}^g)}{\sum_{j \in \mathcal{L} \setminus \Phi} \exp(-f_{j\phi}^g)} \quad (9)$$

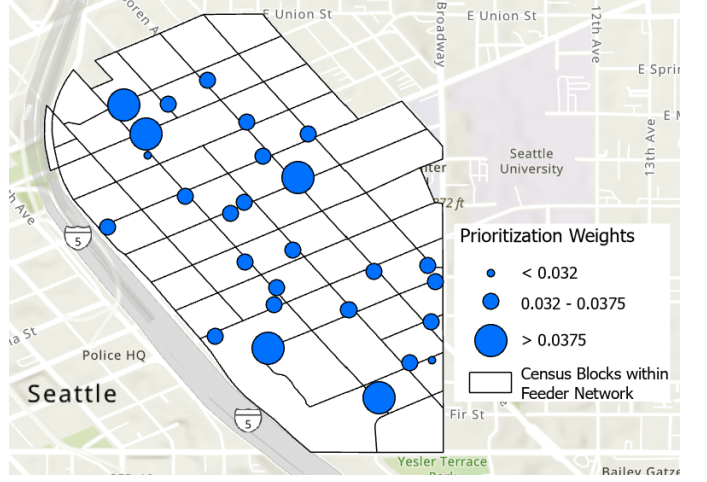


Fig. 3. Spatial distribution of candidate locations in selected feeder in downtown Seattle, with node sizes proportional to their prioritization weights.

III. GRID-ECO OPTIMIZATION MODEL FORMULATION

Given feeder EV charging demand, and candidate locations with appropriate priority weights, we formulate a constrained MINLP optimization problem to find the optimal locations and the number of chargers.

A. Objective Function

The objective of Grid-ECO is to maximize user access to charging stations by deploying the maximum number of chargers across the most candidate locations while meeting *at least* the charging demand D from the transportation model. Mathematically, the objective function is:

$$f(\mathbf{x}, \mathbf{z}) = \sum_{l \in \mathcal{L}} \sum_{p \in \Phi} w_{lp} \cdot x_{lp} \cdot z_{lp} \quad (10)$$

The parameter w_{lp} represents the priority of adding a charger at candidate location l and phase p . The binary decision variable $x_{lp} \in \{0, 1\}$ equals 1 if we add a charging station at node l and phase p , and 0 otherwise, whereas z_{lp} represents the number of chargers in location (l,p) .

B. Constraints

Grid Physics Constraint

We enforce grid physics by placing charging stations to satisfy Kirchhoff's current law (KCL) at every node. To model AC network

constraints, we use a three-phase equivalent circuit [19] and express power flow with the current-voltage (*IV*) formulation. This is equivalent to the current injection method for three-phase power flow [20]. We prefer the *IV* formulation over the *PQV* formulation because it allows for *exact* bilinear formulation of the problem.

For notational clarity, we omit three-phase transformers, shunts, switches, regulators, and fuses but include them in the implementation.

We model the current injection (\tilde{I}) for loads and chargers using Ohm's law in terms of surrogate conductance (G), susceptance (B), and voltage (\tilde{V}) as:

$$\tilde{I} = (G + jB)\tilde{V} \quad (11)$$

The AC network constraints in rectangular form are given by equations (12)–(16).

For all $p \in \Phi$ and $k \in \mathcal{K}$:

Real KCL constraints

$$I_{kp}^{r,load} + I_{kp}^{r,line} + I_{kp}^{r,ch} = 0 \quad (12)$$

where,

$$I_{kp}^{r,load} - (G_{kp}^{load}V_{kp}^r - B_{kp}^{load}V_{kp}^i) = 0 \quad (13a)$$

$$I_{kp}^{r,line} - \left(\sum_{j \in \mathcal{K} \setminus \Phi} \sum_{\phi} G_{kj,p\phi}^{line} V_{kj,\phi}^r - B_{kj,p\phi}^{line} V_{kj,\phi}^i \right) = 0 \quad (13b)$$

$$I_{kp}^{r,ch} - (G_{kp}^{ch}V_{kp}^r - B_{kp}^{ch}V_{kp}^i) = 0 \quad (13c)$$

Imaginary KCL constraints

$$I_{kp}^{i,load} + I_{kp}^{i,line} + I_{kp}^{i,ch} = 0 \quad (14)$$

where,

$$I_{kp}^{i,load} - (G_{kp}^{load}V_{kp}^i + B_{kp}^{load}V_{kp}^r) = 0 \quad (15a)$$

$$I_{kp}^{i,line} - \left(\sum_{j \in \mathcal{K} \setminus \Phi} \sum_{\phi} G_{kj,p\phi}^{line} V_{kj,\phi}^i + B_{kj,p\phi}^{line} V_{kj,\phi}^r \right) = 0 \quad (15b)$$

$$I_{kp}^{i,ch} - (G_{kp}^{ch}V_{kp}^i + B_{kp}^{ch}V_{kp}^r) = 0 \quad (15c)$$

We express the conductance and susceptance of loads and chargers in terms of nonlinear relationships of active and reactive power:

$$G_{kp}^{load} - \frac{P_{kp}^{load}}{(V_{kp}^r)^2 + (V_{kp}^i)^2} = 0 \quad (16a)$$

$$B_{kp}^{load} + \frac{Q_{kp}^{load}}{(V_{kp}^r)^2 + (V_{kp}^i)^2} = 0 \quad (16b)$$

For all candidate locations $k \in \mathcal{L}$:

$$G_{kp}^{ch} - \frac{P_{kp}^{ch}}{(V_{kp}^r)^2 + (V_{kp}^i)^2} = 0 \quad (17a)$$

$$B_{kp}^{ch} + \frac{Q_{kp}^{ch}}{(V_{kp}^r)^2 + (V_{kp}^i)^2} = 0 \quad (17b)$$

Equations (12) and (14) enforce KCL at each node k and phase p . The charger currents $I_{kp}^{r,ch}$ and $I_{kp}^{i,ch}$ activate only if $k \in \mathcal{L}$; otherwise, they are zero. Equations (13a), (13c), (15a), and (15c) model the nonlinear currents through loads and chargers.

Equations (13b) and (15b) model the linear line currents. Equations (16a)–(17b) compute conductance and susceptance in terms of active/reactive power and voltages. Active and reactive power for loads are data, while for chargers, they are decision variables.

Grid Limit Constraint

We enforce operational limits on the grid after placing charging stations to maintain system reliability. Specifically, we constrain node voltage magnitudes within specified bounds and ensure that transformer currents do not exceed their thermal ratings. Line thermal limits and other equipment-specific limits are incorporated analogously. Voltage limit:

$$(V_{kp}^L)^2 \leq (V_{kp}^r)^2 + (V_{kp}^i)^2 \leq (V_{kp}^U)^2, \quad \forall p \in \Phi, \forall k \in \mathcal{K} \quad (18)$$

Transformer current limit:

$$(I_{\tau}^r)^2 + (I_{\tau}^i)^2 \leq (I_{\tau}^{rat})^2, \quad \forall \tau \in \mathcal{T} \quad (19)$$

Charger Demand Constraint

We want to ensure that at least D number of chargers are installed in the selected feeder.

$$D - \sum_{l \in \mathcal{L}} \sum_{p \in \Phi} z_{lp} \leq 0 \quad (20)$$

Furthermore, parking availability is limited; therefore, constraint (21) ensures that charger deployment respects physical limits, as defined by the minimum and maximum allowable chargers, z_{lp}^L and z_{lp}^U .

$$x_{lp} z_{lp}^L - z_{lp} \leq 0, \quad \forall p \in \Phi, \forall l \in \mathcal{L} \quad (21a)$$

$$z_{lp} - x_{lp} z_{lp}^U \leq 0, \quad \forall p \in \Phi, \forall l \in \mathcal{L} \quad (21b)$$

Since z_{lp} is a positive integer, constraint (21) also ensures that if the location is not feasible ($x_{lp} = 0$) for placement of a charging station, then no chargers are installed at that location.

The active power consumed by an EVCS equals the total power drawn by all chargers deployed at that location, given by the number of installed chargers multiplied by the charger power rating $P^{ch, rat}$:

$$P_{lp}^{ch} - z_{lp} P^{ch, rat} = 0 \quad (22)$$

Additionally, we want enforce power factor (pf) for all charging stations:

$$Q_{lp}^{ch} - P_{lp}^{ch} \cdot \tan(\cos^{-1}(pf)) = 0, \quad \forall p \in \Phi, \forall l \in \mathcal{L} \quad (23)$$

Budget Constraint

We ensure that the total cost, including land acquisition (C_{lp}^{EVCS}) and charger installation (C^{ch}), remains within the available budget (C).

$$\sum_{l \in \mathcal{L}} \sum_{p \in \Phi} (C_{lp}^{EVCS} x_{lp} + C^{ch} z_{lp}) \leq C \quad (24)$$

Anti-Clustering Constraint

To prevent charging stations from clustering within the same census block, we enforce a spatial separation among candidate locations based on a predefined service radius (R). As illustrated in Fig. 4, if the service areas of two candidate locations intersect, i.e., the distance between locations (d_{lj}) is less than twice the service radius ($2R$), then at most one charging station can be installed at those locations. This condition is enforced by the following constraint:

$$x_l + x_j \leq 1, \quad \text{if } l \neq j \text{ and } d_{lj} \leq 2R, \quad \forall l, j \in \mathcal{L}. \quad (25)$$

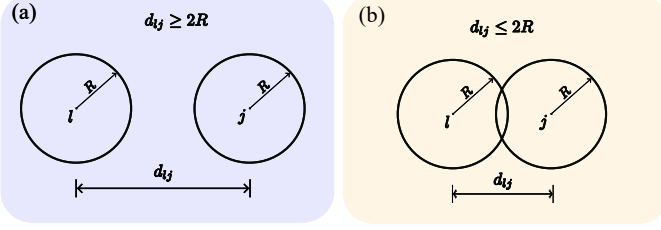


Fig. 4. Illustration of the service radius for two charging stations. In (a), the service radii do not intersect, and the constraint is inactive. In (b), the service radii intersect, activating the anti-clustering constraint.

We compute the service radius R following [10], where it is defined as the maximum distance an EV user is willing to travel to reach a charging station. To evaluate the distance between two candidate locations, we use the Haversine formula [21], which accounts for the Earth's curvature and computes distances based on latitude and longitude coordinates. The Haversine distance is given by:

$$a = \sin^2\left(\frac{\Delta\text{lat}}{2}\right) + \cos(\text{lat}_l)\cos(\text{lat}_j)\sin^2\left(\frac{\Delta\text{long}}{2}\right), \quad (26)$$

$$c = 2 \cdot \text{atan}2(\sqrt{a}, \sqrt{1-a}), \quad (27)$$

$$d_{lj} = r \cdot c, \quad (28)$$

where lat_l and lat_j denote the latitudes of locations l and j , respectively, and long_l and long_j denote their longitudes. Here, $\Delta\text{lat} = \text{lat}_j - \text{lat}_l$ and $\Delta\text{long} = \text{long}_j - \text{long}_l$. The parameter r represents the mean radius of the Earth, approximately 6,371 km.

Combining all constraints and the objective function, the optimization model is formulated as a Mixed-Integer Nonlinear Program (MINLP):

$$\mathbf{P}_{\text{minlp}}: \max f(\mathbf{x}, \mathbf{z}) \quad (29a)$$

$$\text{s.t. } g(\mathbf{y}) = 0 \quad (29b)$$

$$h(\mathbf{x}, \mathbf{y}, \mathbf{z}) \leq 0 \quad (29c)$$

$$\mathbf{y}^L \leq \mathbf{y} \leq \mathbf{y}^U \quad (29d)$$

$$\mathbf{x} \in \{0,1\}^{n_x} \quad (29e)$$

$$\mathbf{z} \in \mathbb{Z}_+^{n_x} \quad (29f)$$

In (29), the objective function (29a) is defined by (10). Constraint (29b) represents the grid physics constraints given in (12)–(17), where \mathbf{y} denotes the vector of all AC network state variables. Constraint (29c) captures the inequality constraints, including grid operating limits (equations (18)–(19)), charger demand constraints (equations (20)–(23)), the budget constraint (24), and the service radius constraint (25), where \mathbf{x} and \mathbf{z} are the vector of candidate locations and vector of number of chargers deployed at those locations. Constraint (29d) bounds the state variables. The AC network equations introduce nonlinearity and non-convexity into (29). Additionally, the decision variables governing EVCS placement and charger counts, represented in (29e) and (29f), further increase the complexity of the formulation, making the original optimization problem a non-convex MINLP.

IV. GRID-ECO SOLUTION METHODOLOGY

State-of-the-art solvers cannot directly solve $\mathbf{P}_{\text{minlp}}$ in Section III while providing certifiable guarantees on solution quality. Existing

studies ([11], [12], [13]) typically circumvent $\mathbf{P}_{\text{minlp}}$ either by deriving convex relaxations of the nonlinear AC network constraints while retaining the discrete variables and solving the resulting MILP, or by relaxing the discrete variables to obtain an NLP that can be solved using local solvers. However, these relaxations may yield solutions whose quality cannot be certified, and that may be technically infeasible for real-world grid operations.

Recent advancements in global solvers such as Gurobi and BARON can solve a certain class of nonconvex problems, including MIBLPs, to global or near-global optimality, as measured by the optimality gap. For MIBLPs, these solvers use the spatial branch-and-bound (sBnB) algorithm [22] to handle nonconvexities. In the $\mathbf{P}_{\text{minlp}}$ problem considered in this work, the nonlinearity arises from the AC network constraints. We show how these AC network constraints can be exactly reformulated as bilinear constraints by introducing lifting variables, following the approach presented in [16] and further discussed in Section IV-A. Building on our prior work, this paper extends [16] to evaluate the effectiveness of the sBnB algorithm in solving bilinear problems with discrete decision variables, i.e., MIBLPs, to near-zero optimality gap. As illustrated in

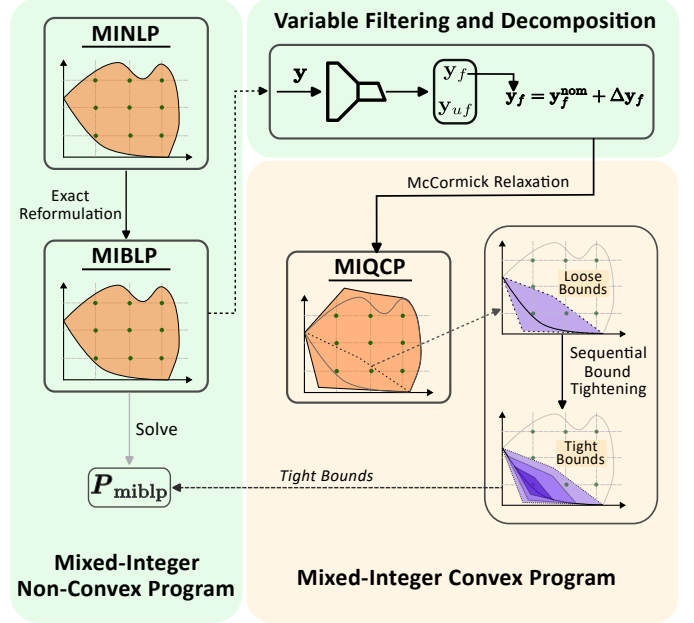


Fig. 5. Overview of the Grid-ECO solution methodology for solving $\mathbf{P}_{\text{minlp}}$ to near-zero optimality gap.

Fig. 5, we first exactly reformulate the original MINLP as an MIBLP, then apply variable filtering and decomposition, followed by convex relaxation of the AC network constraints and sequential bound tightening to solve the resulting MIBLP. Our objective is to assess whether this strategy enables achieving near-zero optimality gaps.

A. Reformulation as the Mixed-Integer Bilinear Program

We exactly reformulate the original MINLP as MIBLP. In particular, the nonlinear constraints (16)–(17) require bilinear reformulation, which we achieve by introducing the lifting variable V_{kp}^{sq} defined in (30).

$$V_{kp}^{sq} = (V_{kp}^r)^2 + (V_{kp}^i)^2 \quad (30)$$

Then, as an example, the bilinear reformulation of (16a) is given by (31):

$$G_{kp}^{load}V_{kp}^{sq} - P_{kp}^{load} = 0 \quad (31)$$

Using the same approach, we reformulate the remaining nonlinear equations ((16b)–(17b)) into bilinear form. The resulting MIBLP model in (32) is an exact reformulation of the original MINLP problem and preserves its feasible region.

$$\mathbf{P}_{\text{miblp}}: \max f(\mathbf{x}, \mathbf{z}) \quad (32a)$$

$$\text{s.t. } g_{\text{miblp}}(\mathbf{y}, \mathbf{s}) = 0 \quad (32b)$$

$$h_{\text{miblp}}(\mathbf{x}, \mathbf{y}, \mathbf{z}, \mathbf{s}) \leq 0 \quad (32c)$$

$$\mathbf{y}^L \leq \mathbf{y} \leq \mathbf{y}^U \quad (32d)$$

$$s_k = y_i y_j \quad \forall k \in BL \quad (32e)$$

$$\mathbf{x} \in \{0,1\}^{n_x} \quad (32f)$$

$$\mathbf{z} \in \mathbb{Z}_+^{n_x} \quad (32g)$$

Here, s_k denotes the k^{th} bilinear term, where each $s_k = y_i y_j$ for $(i, j) \in BL$, and the vector \mathbf{s} contains all such bilinear terms, i.e., $\mathbf{s} = \{s_k \mid k \in BL\}$. The equality constraint (32b) includes the linear and bilinear AC network constraints. The inequality constraint (32c) represents the bilinear grid limit constraints, along with other linear constraints such as charging capacity, budget, and service radius (anti-clustering of EVCS).

The spatial branch-and-bound algorithm can solve the $\mathbf{P}_{\text{miblp}}$ problem to near-zero optimality gap by dividing the root node solution space into smaller subspaces (child nodes) and solving relaxed problems, and pruning subproblems when possible [22]. The algorithm often explores many subproblems before reaching the global optimum. For each subproblem, the algorithm applies convex relaxation and bound tightening, solves the relaxed and the nonlinear problem, and searches for an integer-feasible solution using the standard branch-and-bound algorithm.

For solving large-scale $\mathbf{P}_{\text{miblp}}$ problem using off-the-shelf Gurobi solver, if no bounds or loose bounds are given, the solver often uses their presolving strategy to achieve bounds for the variables, and we find these bounds are often loose, so the sBnB algorithm needs to explore large uninformative feasible space to find a solution (shown in Fig. 6 (a)), which makes the off-the-self solver impractical to solve MINLP [23] as it degrades the computational performance. However, if we provide tight bounds on the bilinear variables, knowing a priori that the global solution lies within these bounds, we can significantly shrink the feasible space (as shown in Fig. 6(b)) and improve the performance of the sBnB algorithm.

To obtain these tight bounds, we extend the presolving strategy introduced in [16]. This strategy applies variable filtering and decomposition, along with a bound-tightening method. We discuss these techniques in Subsections IV-B and IV-C, respectively.

B. Variable Filtering and Decomposition

Large-scale MIBLP problems contain a large number of bilinear variables. Applying sequential bound tightening (SBT) to all variables makes the presolving strategy slow. To address this issue, we identify and filter independent variables (denoted as $\mathbf{y}_f \subset \mathbf{y}$), apply bound tightening only to them, and then compute bounds for unfiltered dependent variables (denoted as $\mathbf{y}_{uf} \subset \mathbf{y}$) in a post-processing step, as discussed in [16].

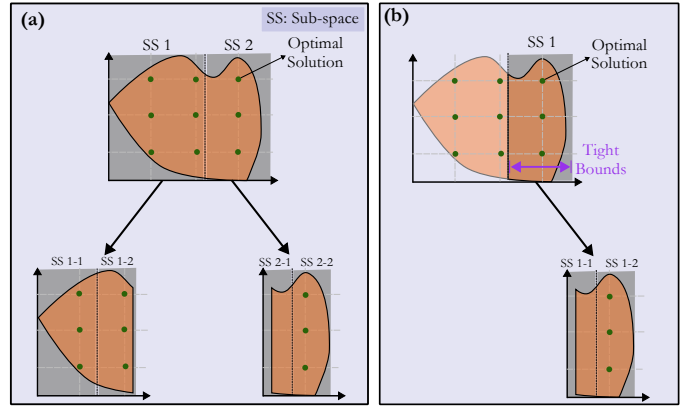


Fig. 6. The figure shows the branching process of the spatial branch-and-bound algorithm. Fig. (a) shows the traditional method, which explores all branches. Fig. (b) shows the Grid-ECO method, where the algorithm explores fewer branches due to a smaller feasible space resulting from tighter variable bounds.

For example, in the bilinear equation (31), the variables G_{kp}^{load} and V_{kp}^{sq} are dependent variables (i.e., $G_{kp}^{load}, V_{kp}^{sq} \subset \mathbf{y}_{uf}$). From (30), the variable V_{kp}^{sq} depends on V_{kp}^r and V_{kp}^i (i.e., $V_{kp}^r, V_{kp}^i \subset \mathbf{y}_{uf}$). The variable G_{kp}^{load} can be expressed using (16a) and (30) as

$$G_{kp}^{load} = \frac{P_{kp}^{load}}{V_{kp}^{sq}} \quad (33)$$

Equation (33) shows that G_{kp}^{load} depends on V_{kp}^{sq} , and V_{kp}^{sq} depends on V_{kp}^r and V_{kp}^i . Therefore, tightening the bounds on V_{kp}^r and V_{kp}^i allows us to derive tight bounds for V_{kp}^{sq} and G_{kp}^{load} . By performing bound tightening only on independent variables, we significantly reduce the number of variables involved in the tightening process, which accelerates the presolving strategy.

We decompose the filtered variables into nominal values ($\mathbf{y}_f^{\text{nom}}$) and deviation components ($\Delta \mathbf{y}_f$) as represented in equation (34), where base values are known parameters and deviations are optimization variables. This decomposition allows us to assign small, well-defined upper and lower bounds to the deviation terms. Moreover, we can apply the same bounds across all phases, simplifying the formulation.

$$\mathbf{y}_f = \mathbf{y}_f^{\text{nom}} + \Delta \mathbf{y}_f \quad (34)$$

For example, we can express the real and imaginary parts of the voltage at node k and phase p as

$$V_{kp}^r = V_k \cdot \cos(\theta_p) + \Delta V_{kp}^r, \quad (35a)$$

$$V_{kp}^i = V_k \cdot \sin(\theta_p) + \Delta V_{kp}^i \quad (35b)$$

Here, V_k is the nominal voltage at bus k , and θ_p is the nominal phase angle, taking values $0, -2\pi/3$, and $2\pi/3$ radians for phases $p \in \Phi$. The terms ΔV_{kp}^r and ΔV_{kp}^i represent the deviations of the real and imaginary parts of the voltage from nominal.

With the decomposition, the bilinear expression in (13a) is reformulated in (35) as

$$I_{kp}^{r,load} - \underbrace{\left[G_{kp}^{load} \Delta V_{kp}^r - B_{kp}^{load} \Delta V_{kp}^i + \right]}_{\text{Bilinear}} + \underbrace{\left[\left(G_{kp}^{load} V_k \cos(\theta_p) - B_{kp}^{load} V_k \sin(\theta_p) \right) \right]}_{\text{Linear}} = 0 \quad (36)$$

The bilinear terms $G_{kp}^{load} \Delta V_{kp}^r$ and $B_{kp}^{load} \Delta V_{kp}^i$ in (36) are relaxed using the McCormick envelope for bound tightening. See Section IV-C and shown in (37).

C. Convex Relaxation of MIBLP and Bound Tightening

We apply the SBT method proposed in [24], which iteratively solves the bound contraction algorithm introduced in [25] to obtain tight variable bounds by progressively shrinking the feasible region of the $\mathbf{P}_{\text{miblp}}$ problem. In SBT, we construct an outer approximation of the bilinear constraints using the McCormick relaxation [26] and iteratively solve the problem defined in (38).

The McCormick envelope for a generic bilinear term $y = v_1 v_2$ is denoted by the operator $M_c(\cdot)$ and is defined as:

$$M_c(y, [v_1, v_2]) = \begin{cases} v_1^U v_2 + v_1 v_2^U - v_1^U v_2^U - y \leq 0, \\ v_1^L v_2 + v_1 v_2^L - v_1^L v_2^L - y \leq 0, \\ y - v_1^U v_2 - v_1 v_2^L + v_1^U v_2^L \leq 0, \\ y - v_1^L v_2 - v_1 v_2^U + v_1^L v_2^U \leq 0 \end{cases} \quad (37)$$

where v_1^U , v_2^U , v_1^L , and v_2^L denote the upper and lower bounds of the bilinear variables.

After filtering and decomposing the variables into their nominal and deviation components, we simultaneously replace each filtered variable by the sum of its nominal value and deviation factor, as shown in equation (36). Applying this transformation to all bilinear terms in the $\mathbf{P}_{\text{miblp}}$ problem yields a convex relaxation of the bilinear constraints, thereby relaxing the MIBLP to an MIQCP.

The conversion of the MIBLP to an MIQCP enables the implementation of Sequential Bound Tightening (SBT), as outlined in Algorithm 1, to compute tight bounds on the deviation components of the filtered variables, Δy_f . The algorithm takes as input initial loose bounds on Δy_f and a bound-tightening tolerance ϵ .

Before applying SBT, we impose an objective bound using a locally optimal solution, as shown in (38c). Specifically, we relax the integer variables in $\mathbf{P}_{\text{minlp}}$ and solve the resulting problem as an NLP to obtain a local solution with objective value $f_{\text{nlp}}(\mathbf{x}^*, \mathbf{z}^*)$. The key modification we introduce to the original SBT algorithm in [24] lies in this objective-bounding step. Since our formulation is a maximization problem, we enforce a lower bound on the objective, derived from the local solver, rather than the upper bound typically used for minimization problems.

After initializing the bounds for all deviation variables, SBT starts by solving, for each variable $\Delta y_{f,i}$, two independent optimization problems in parallel: one minimizing $\Delta y_{f,i}$ and the other maximizing $\Delta y_{f,i}$. This process yields the tightest lower and upper bounds for each $\Delta y_{f,i}$ by iteratively solving (38) until the difference between the bounds falls below the prescribed tolerance ϵ . Constraint (38d) represents the affine AC network equations. Constraint (38e) captures the convex grid limit constraints and other linear constraints originally defined in (29c). Constraint (38f) enforces the McCormick envelopes for the bilinear terms. Constraint (38g) enforces bounds on the unfiltered variables, while constraint (38h) bounds the deviation components of the filtered variables.

V. CASE STUDIES

In this section, we evaluate the performance of Grid-ECO on two study regions within the City of Seattle: a downtown area and a residential neighborhood. First, we compare Grid-ECO's ability to solve

Algorithm 1: Sequential Bound Tightening on Δy_f

Input: $\Delta y_f^L, \Delta y_f^U, \epsilon$
1 Solve: $\mathbf{P}_{\text{minlp}}$ with local solver by relaxing integer constraints ((29e)–(29f)) to obtain $f_{\text{nlp}}(\mathbf{x}^*, \mathbf{z}^*)$
2 Initialize: $\Delta y_f^l \leftarrow \Delta y_f^L$, $\Delta y_f^u \leftarrow \Delta y_f^U$
3 Set: $(\Delta y_f)_{\text{prev}}^l \leftarrow 0$, $(\Delta y_f)_{\text{prev}}^u \leftarrow 0$
4 while $\|\Delta y_f^l - (\Delta y_f)_{\text{prev}}^l\|_2 > \epsilon$ and $\|\Delta y_f^u - (\Delta y_f)_{\text{prev}}^u\|_2 > \epsilon$ **do**
5 $(\Delta y_f)_{\text{prev}}^l \leftarrow \Delta y_f^l$, $(\Delta y_f)_{\text{prev}}^u \leftarrow \Delta y_f^u$
6 **foreach** $\Delta y_{f,i} \in \Delta y_f$ **do**
7 **Solve** in parallel:

$$\Delta y_{f,i}^{l*} := \min(\Delta y_{f,i}) \quad (38a)$$

$$\Delta y_{f,i}^{u*} := \max(\Delta y_{f,i}) \quad (38b)$$

subject to

$$f(\mathbf{x}, \mathbf{z}) \geq f_{\text{nlp}}(\mathbf{x}^*, \mathbf{z}^*) \quad (38c)$$

$$g_{\text{aff}}(\mathbf{y}_{uf}, \Delta y_f, \mathbf{s}) = 0 \quad (38d)$$

$$h_{\text{cvx}}(\mathbf{y}_{uf}, \Delta y_f, \mathbf{x}, \mathbf{z}, \mathbf{s}) \leq 0 \quad (38e)$$

$$h_{\text{mc}}(\mathbf{y}_{uf}, \Delta y_f, \mathbf{s}) \leq 0 \quad (38f)$$

$$\mathbf{y}_{uf}^l \leq \mathbf{y}_{uf} \leq \mathbf{y}_{uf}^u \quad (38g)$$

$$(\Delta y_f)_{\text{prev}}^l \leq \Delta y_f \leq (\Delta y_f)_{\text{prev}}^u \quad (38h)$$

$$\mathbf{x} \in \{0,1\}^{n_x} \quad (38i)$$

$$\mathbf{z} \in \mathbb{Z}_+^{n_z} \quad (38j)$$
8 $\Delta y_f^l \leftarrow (\Delta y_f)_{\text{prev}}^{l*}$, $\Delta y_f^u \leftarrow (\Delta y_f)_{\text{prev}}^{u*}$
9 **Update** $(\mathbf{y}_{uf}^l, \mathbf{y}_{uf}^u)$
Output: tightened bounds: $\Delta y_f^l, \Delta y_f^u, \mathbf{y}_{uf}^l, \mathbf{y}_{uf}^u$

the $\mathbf{P}_{\text{miblp}}$ using the off-the-shelf Gurobi sBnB algorithm, denoted as MIBLP in the *Approach* column of Table V. Second, we solve the $\mathbf{P}_{\text{miblp}}$ using our proposed presolving routine, denoted as S-MIBLP.

A. Parameter Settings

For the transportation model, we use multiple data sources ([27], [28], [29]) to capture parking availability, demographic characteristics, and EV adoption rates in Seattle, WA. The policy weighting parameter α is set to 0.85, representing a balanced emphasis between efficiency-driven utilization and equity-oriented accessibility [17]. The city-wide total chargers across all census blocks b is set to 3,085, which ensures a deployment target of five charging ports per 1,000 households across the study area.

For the grid model, we use an average power rating of 7.2 kW for Level-2 chargers [30] with a power factor of 0.985 [31]. The average installation cost per charger is set to \$8,600 [32]. Due to the unavailability of actual land acquisition costs, we assume costs based on parking availability. The detailed land acquisition costs for each candidate location used in these case studies are provided in the repository [33]. The total installation budget is set to \$2.5M for the downtown area and \$2M for the residential neighborhood. These cost and power parameters are used to demonstrate the performance of the optimization model in a real-world urban setting; however, utilities and city planners can adjust them to reflect region-specific economic and operational conditions. To prevent spatial clustering, the service radius is set to 100 m for the

downtown area and 200 m for the residential neighborhood.

We solve the MIBLP, S-MIBLP, and MILP formulations using the Gurobi solver [34] (version 13.0.0), and we solve the NLP formulation using the IPOPT solver (version 3.14.17) [35]. All optimization runs are performed on a high-performance computing (HPC) cluster equipped with an AMD EPYC 9654 96-core processor with 192 physical cores and 192 logical threads [36].

B. Study Region

1) Case 1: Downtown

We conduct a case study on a dense urban downtown region. The selected study area contains seven census blocks with EV charging demand, as shown in Fig. 1 (right, zoomed view). Based on the demand estimation described in Section II-B, the charging demand across these census blocks ranges from 2 to 28 chargers, totaling 71 required chargers within the region. We overlay the representative synthetic feeder R3-12-47-2 [37] onto the selected study region to model the downtown distribution feeder. Following the location selection and prioritization procedure described in Section II-C, the framework first identifies 27 candidate EVCS locations and prioritizes them accordingly, as shown in Fig. 3.

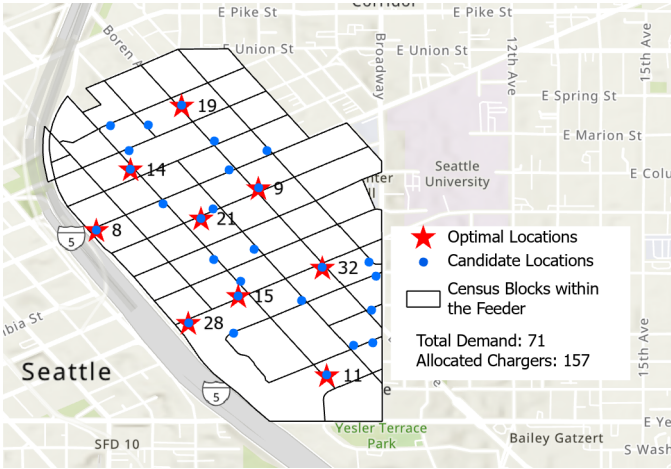


Fig. 7. Distribution of candidate locations and the optimal locations in the selected downtown region. Blue circles denote candidate locations, and red stars indicate the optimal locations selected by the model.

Fig. 7 presents the Grid-ECO results obtained using the S-MIBLP approach, showing the optimal EVCS locations overlaid on the set of candidate locations. The numbers in the figure indicate the optimal number of chargers deployed at each station. Of the 27 candidate locations, the model selects nine locations, providing capacity for 157 chargers and satisfying the minimum charging demand requirement. The solution is global or near-global, as the reported optimality gap is 0.0000%.

2) Case 2: Residential Neighborhood

We conduct a second case study on a residential neighborhood region characterized by low density and sparse EV charging demand. The residential region has a total charging demand of 149 chargers. We overlay the representative synthetic feeder R1-25-00-1 [37] onto the study area to model the residential distribution feeder. Within this feeder, the framework first identifies eight candidate charging station locations, as shown by the blue circles in Fig. 8.

In Fig. 8, Grid-ECO selects three optimal EVCS locations from

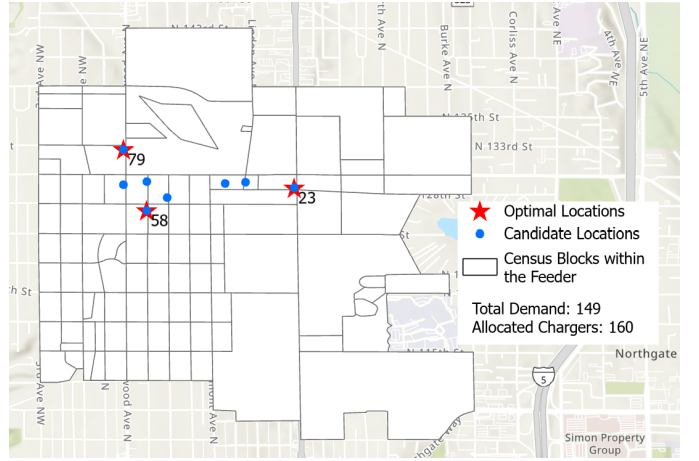


Fig. 8. Candidate charging station locations and the optimized selection for the residential feeder.

the eight candidate locations, providing capacity to serve 160 vehicles during the peak hour and satisfying the minimum charging demand requirement. The solution is global or near-global, as the reported optimality gap is 0.0000%.

C. Comparison against the State-of-the-art Algorithm

We compare the performance of the Gurobi solver in solving P_{miblp} with i) algorithm with our presolving routine in Section IV - S-MIBLP and ii) without - MIBLP. For comparison, we report the objective value (Objective), the optimality gap percentage (Gap (%)), and the number of nodes (child nodes) explored by the sBnB algorithm (# sBnB Nodes) in Table V. In Table V, # Feeder Nodes denotes the number of electrical buses in the distribution feeder.

For the downtown case with a feeder of 863 buses, the MIBLP could not find any feasible solution within approximately 167 hours (reached time limit). In contrast, S-MIBLP found the solution in approximately 57 minutes, exploring 1760 sBnB nodes with a 0.000% optimality gap. For the residential neighborhood feeder with 830 buses, MIBLP solved the problem in approximately 6 hours, exploring 43,459 sBnB nodes, whereas S-MIBLP solved it in 1 hour and 32 minutes while exploring only 1,381 nodes. Both approaches achieved a 0.000% optimality gap and allocated the same number of EVCS locations and chargers.

VI. CONCLUSION

In this paper, we introduced Grid-ECO, an optimization framework for allocating and deploying EV chargers while satisfying AC network constraints. By reformulating the original non-convex MINLP as MIBLP, the Grid-ECO solution methodology achieves exact solutions with significant computational improvements over off-the-shelf methods. The key findings of this work are summarized below:

- Grid-ECO accurately mapped census-level EV charger demand to the distribution feeder and deployed chargers to satisfy the estimated demand.
- The framework solved all MINLP tested cases exactly with an optimality gap of 0.0000%, ensuring a global or near-global solution.
- Grid-ECO successfully solved Case 1 (downtown Seattle feeder) in 3.5k seconds, whereas the off-the-shelf Gurobi solver failed to find a feasible solution within 600k seconds, demonstrating the robustness and efficiency of the proposed

TABLE V
COMPARISON OF TWO SOLUTION APPROACHES FOR SOLVING P_{MIBLP} IN TWO STUDY REGIONS

| Case | Feeder | # Feeder Nodes | Approach | Objective | Time (s) | # sBnB Nodes | Gap (%) | Total EVCS Locations | Total Chargers Deployed |
|---------------------------|------------|----------------|------------------|--------------------|---------------------|---------------|------------------|----------------------|-------------------------|
| Downtown | R3-12-47-2 | 863 | MIBLP S-MIBLP | — 5.8001 | 601200 3458.31 | — 1760 | 0.0000 | — 9 | — 157 |
| Residential Neighbourhood | R1-25-00-1 | 830 | MIBLP S-MIBLP | 20.4494 20.4494 | 20782.35 5533.68 | 43459 1381 | 0.0000 0.0000 | 3 3 | 160 160 |

approach.

- For Case 2, representing a residential Seattle feeder, in comparison to the off-the-shelf Gurobi sBnB algorithm, Grid-ECO reduced solution time by up to 73% and sBnB node exploration by up to 97%.

VII. ACKNOWLEDGEMENT

This research was supported by the U.S. Department of Energy Vehicle Technologies Office (Grant No. DEEE0010640) and the Alfred P. Sloan Foundation (Grant No. 2024-22563).

REFERENCES

- [1] International Energy Agency, “Global ev outlook 2025: Expanding sales in diverse markets,” International Energy Agency, Report, 2025, cC BY 4.0. [Online]. Available: <https://iea.blob.core.windows.net/assets/0aa4762f-c1cb-4495-987a-25945d6de5e8/GlobalEVOutlook2025.pdf>
- [2] M. Muratori and T. Mai, “The shape of electrified transportation,” *Environmental Research Letters*, vol. 16, no. 1, p. 011003, Dec. 2020. [Online]. Available: <http://dx.doi.org/10.1088/1748-9326/abcb38>
- [3] B. Yang, J. Li, H. Shu, Z. Cai, B. Tang, X. Huang, and M. Zhu, “Recent advances of optimal sizing and location of charging stations: A critical overview,” *International Journal of Energy Research*, vol. 46, no. 13, pp. 17899–17925, 2022.
- [4] J. Jordán, J. Palanca, P. Martí, and V. Julian, “Electric vehicle charging stations emplacement using genetic algorithms and agent-based simulation,” *Expert Systems with Applications*, vol. 197, p. 116739, 2022.
- [5] Y. S. Liu, M. Tayarani, F. You, and H. O. Gao, “Bayesian optimization for battery electric vehicle charging station placement by agent-based demand simulation,” *Applied Energy*, vol. 375, p. 123975, 2024.
- [6] H. Moon, S. Y. Park, C. Jeong, and J. Lee, “Forecasting electricity demand of electric vehicles by analyzing consumers’ charging patterns,” *Transportation Research Part D: Transport and Environment*, vol. 62, pp. 64–79, 2018.
- [7] S. Wang, C. Zhuge, C. Shao, P. Wang, X. Yang, and S. Wang, “Short-term electric vehicle charging demand prediction: A deep learning approach,” *Applied Energy*, vol. 340, p. 121032, 2023.
- [8] Z. Yi, B. Chen, X. C. Liu, R. Wei, J. Chen, and Z. Chen, “An agent-based modeling approach for public charging demand estimation and charging station location optimization at urban scale,” *Computers, Environment and Urban Systems*, vol. 101, p. 101949, 2023.
- [9] A. Agarwal, A. Pandey, and L. Pillegi, “Continuous switch model and heuristics for mixed-integer problems in power systems,” *arXiv preprint arXiv:2206.14510*, 2022.
- [10] Z. Liu, F. Wen, and G. Ledwich, “Optimal planning of electric-vehicle charging stations in distribution systems,” *IEEE transactions on power delivery*, vol. 28, no. 1, pp. 102–110, 2012.
- [11] J. F. Franco, M. J. Rider, and R. Romero, “A mixed-integer linear programming model for the electric vehicle charging coordination problem in unbalanced electrical distribution systems,” *IEEE Transactions on Smart Grid*, vol. 6, no. 5, pp. 2200–2210, 2015.
- [12] R. Xie, W. Wei, M. E. Khodayar, J. Wang, and S. Mei, “Planning fully renewable powered charging stations on highways: A data-driven robust optimization approach,” *IEEE transactions on transportation electrification*, vol. 4, no. 3, pp. 817–830, 2018.
- [13] Q. Cui, Y. Weng, and C.-W. Tan, “Electric vehicle charging station placement method for urban areas,” *IEEE Transactions on Smart Grid*, vol. 10, no. 6, pp. 6552–6565, 2019.
- [14] X. Zhu, B. Mather, and P. Mishra, “Grid impact analysis of heavy-duty electric vehicle charging stations,” in *2020 IEEE Power & Energy Society Innovative Smart Grid Technologies Conference (ISGT)*. IEEE, 2020, pp. 1–5.
- [15] X. Zhao, C. Zhao, and G. Jia, “Grid-aware on-route fast-charging infrastructure planning for battery electric bus with equity considerations: A case study in south king county,” *arXiv preprint arXiv:2309.07422*, 2023.
- [16] B. Panthee and A. Pandey, “Solving three-phase ac infeasibility analysis to near-zero optimality gap,” *arXiv preprint arXiv:2508.15937*, 2025.
- [17] C. M. S. Lezcano, C. D. Harper, and D. Nock, “Siting for demand and equity: Optimizing level 2 electric vehicle charger placement,” *Journal of Transport Geography*, vol. 128, p. 104369, 2025.
- [18] X. Zhu, J. Wang, D. Mulcahy, D. L. Lubkeman, N. Lu, N. Samaan, and R. Huang, “Voltage-load sensitivity matrix based demand response for voltage control in high solar penetration distribution feeders,” in *2017 IEEE Power & Energy Society General Meeting*. IEEE, 2017, pp. 1–5.
- [19] A. Pandey, M. Jeremimov, M. R. Wagner, D. M. Bromberg, G. Hug, and L. Pillegi, “Robust power flow and three-phase power flow analyses,” *IEEE Transactions on Power Systems*, vol. 34, no. 1, pp. 616–626, 2018.
- [20] P. A. Garcia, J. L. R. Pereira, S. Carneiro, V. M. Da Costa, and N. Martins, “Three-phase power flow calculations using the current injection method,” *IEEE Transactions on power systems*, vol. 15, no. 2, pp. 508–514, 2000.
- [21] E. A. Mohammed, M. H. Qahtan, and A. J. Ali, “Internet of things based real-time electric vehicle and charging stations monitoring system,” *Indonesian Journal of Electrical Engineering and Computer Science*, vol. 27, no. 3, pp. 1661–1669, 2022.
- [22] E. M. B. Smith and C. C. Pantelides, “Global Optimisation of General Process Models,” *Global Optimization in Engineering Design*, pp. 355–386, 1996.
- [23] S. Das Gupta, B. P. Van Parys, and E. K. Ryu, “Branch-and-bound performance estimation programming: A unified methodology for constructing optimal optimization methods,” *Mathematical Programming*, vol. 204, no. 1, pp. 567–639, 2024.
- [24] H. Nagarajan, M. Lu, E. Yamangil, and R. Bent, “Tightening McCormick relaxations for nonlinear programs via dynamic multivariate partitioning,” in *Principles and Practice of Constraint Programming: 22nd International Conference, CP 2016, Toulouse, France, September 5–9, 2016, Proceedings* 22. Springer, 2016, pp. 369–387.
- [25] P. M. Castro, “Tightening piecewise mccormick relaxations for bilinear problems,” *Computers & Chemical Engineering*, vol. 72, pp. 300–311, 2015, a Tribute to Ignacio E. Grossmann. [Online]. Available: <https://www.sciencedirect.com/science/article/pii/S0098135414001069>
- [26] G. P. McCormick, “Computability of global solutions to factorable nonconvex programs: Part i—convex underestimating problems,” *Mathematical programming*, vol. 10, no. 1, pp. 147–175, 1976.
- [27] U. Bureau, “Decennial census demographic and housing characteristics file; 2023,” 2024.
- [28] H. Roers and T. Sherman, “2021 american housing,” 2024.
- [29] U. C. Bureau, “American community survey,” *American Fact Finder*, 2012.
- [30] J. Marsh, “How many watts does an electric car charger use?” EnergySage, December 2023, accessed: 2024-12-20. [Online]. Available: <https://www.energysage.com/electricity/house-watts/how-many-watts-does-an-electric-car-charger-use/>
- [31] NERC Reliability and Security Technical Committee, “Grid friendly EV charging recommendations,” North American Electric Reliability Corporation, Technical Report, 2024. [Online]. Available: https://www.nerc.com/comm/RSTC/Documents/Grid_Friendly_EV_Charging_Recommendations.pdf
- [32] T. Lyons, K.-C. Chu, and J. Smart, “The current state of light-duty electric vehicle supply equipment costs: An assessment of contemporary understanding,” *Sustainability*, vol. 15, no. 23, p. 16373, 2023.
- [33] B. Panthee, “Grid-ECO: Grid Aware Electric Vehicle Charging Stations Placement Optimizer,” <https://github.com/pantheebikram/Grid-ECO>, GitHub, 2026, GitHub repository.
- [34] Gurobi Optimization, LLC, *Gurobi Optimizer Reference Manual*, 2025, version 13.0. [Online]. Available: <https://www.gurobi.com>
- [35] A. Wächter and L. T. Biegler, “On the implementation of an interior-point filter line-search algorithm for large-scale nonlinear programming,” *Mathematical programming*, vol. 106, pp. 25–57, 2006.
- [36] The University of Vermont, “Vermont Advanced Computing Center,” <https://www.uvm.edu/vacc>, 2025.
- [37] K. P. Schneider, Y. Chen, D. P. Chassin, R. G. Pratt, D. W. Engel, and S. E. Thompson, “Modern grid initiative distribution taxonomy final report,” Pacific Northwest National Lab.(PNNL), Richland, WA (United States), Tech. Rep., 2008.